Late-stage coarsening for off-critical quenches: Scaling functions and the growth law

Amitabha Chakrabarti
Department of Physics, Kansas State University, Manhattan, Kansas 66506

Raúl Toral
Instituto de Estudios Avanzados and Department de Física, Consejo Superior de Investigaciones Científicas and Universitat de les Illes Balears, 07071 Palma de Mallorca, Spain

James D. Gunton
Department of Physics, Lehigh University, Bethlehem, Pennsylvania 18015
(Received 15 January 1993)

We carry out a detailed numerical study of the Cahn-Hilliard equation in two dimensions for phase separation in very large systems and for different values of the area fraction ϕ. We present results for the scaling function obtained from the pair-correlation function, the structure factor, and the droplet distribution function. We find that dynamical scaling is satisfied at late times for all of the above functions and for different area fractions. We study how the shape of these scaling functions changes with the area fractions and compare these results with available theoretical predictions. We have also analyzed the growth law for the characteristic domain size for various area fractions. Our analysis of the time dependence of various measures for the characteristic length supports a modified Lifshitz-Slyozov law in which the asymptotic-growth-law exponent is $\frac{1}{3}$ for all area fractions.

PACS number(s): 64.60.My, 64.60.Cn, 64.75.+g

I. INTRODUCTION

When a binary mixture, initially prepared in a homogeneous, high-temperature phase, is suddenly quenched below the coexistence curve, the mixture begins to evolve toward its new energetically favorable segregated phase. In the theoretical approach to the kinetics of these first-order phase transitions [1], a distinction is usually made between two very different mechanisms of evolution following such a quench. The spinodal curve roughly divides the region in the phase diagram where droplets of the minority phase form by nucleation and where the domains form by spinodal decomposition. If the system is quenched between the spinodal curve and the coexistence curve, nuclei of the minority phase are formed and these nuclei subsequently coarsen with time. Inside the spinodal curve the system is unstable against long-wavelength instabilities and evolves by spinodal decomposition. It is, however, well accepted [2–6] that for systems with short-range interactions the spinodal curve does not divide the two regions sharply but merely serves to suggest where each process dominates.

Despite extensive studies, the theoretical understanding of this phase-separation process for quenches to various locations of the phase diagram is still incomplete. However, several important results have been obtained in recent years both by analytical calculations and by large-scale computer simulations. The classical result of Lifshitz and Slyozov (LS) [7] is applicable when the volume fraction of one of the components of the mixture is vanishingly small. In this limit the kinetics of the growth process can be solved analytically and the growth law for the average domain size, $R(t)$ is given by $R(t) \sim t^{1/3}$. Although the Lifshitz-Slyozov theory is only applicable for very dilute systems, it has been argued theoretically [8–12] that a similar $t^{1/3}$ growth law should hold asymptotically at late times for larger values of the volume fraction as well. Another important development in the past several years is the understanding that the late stages of the phase-separation process in various binary mixtures are characterized by one dominant length scale, proportional to the average size of the domains, $R(t)$. Due to the existence of only one length scale, the late-stage evolution of the system can be described in terms of scaling [1,13,14] with $R(t)$. One important question in the area of growth kinetics is, then, whether the growth law and the scaling functions change as one varies the volume fraction ϕ (area fraction in two dimensions) of the minority constituent of the binary mixture.

In this paper we address the above issue by carrying out large-scale computer simulations on the Cahn-Hilliard model [15] of phase separation in two dimensions. In particular, we study how the scaling functions for the scattering intensity and the pair-correlation functions change when the area fraction ϕ of the minority phase is varied. We also study the scaling behavior of the droplet-distribution function, which determines the number of droplets of a given size as a function of time. Most of the theoretical calculations of these quantities are limited to small volume (or area) fractions, since the theories seem to break down for large volume fractions. Numerically, however, studying small volume or area fractions is very difficult due to finite-size limitations. Thus previously it has not been possible to compare the scaling functions found in the analytical studies with those computed in numerical simulations [16]. The small area fractions

accessed in this study allows us to systematically compare the results with various approximate theories in two dimensions. Some of these results have recently been reported by us [17–19]. Here we present the details of this work, including more extensive analysis of the data than presented previously. The outline of the paper is as follows. In Sec. II we introduce the model and discuss the numerical methods used in the study. In Sec. III we present the results for the various scaling functions and compare them with analytical theories whenever possible. In Sec. IV we present the time dependence of the characteristic length, and finally conclude in Sec. V with a brief summary.

II. MODEL AND NUMERICAL METHODS

In the Cahn-Hilliard-Cook theory [15] of the dynamics of first-order phase transitions, one considers a conserved concentration field $\psi(\mathbf{r},t)$ which represents the difference in the local concentration of the two components of the mixture. It is assumed that the time variation of this conserved field is governed by the functional derivative of a free-energy functional given in terms of a Ginzburg-Landau expression plus a thermal noise term as

$$\frac{\partial\psi(\mathbf{r},t)}{\partial t}=M\nabla^2[-b\psi+u\psi^3-K\nabla^2\psi]+\eta(\mathbf{r},t)\ , \qquad (1)$$

where M is the mobility, b, u, and K are the parameters of the model, and the noise variable $\eta(\mathbf{r},t)$ is a Gaussian random variable of mean zero and obeying the correlations

$$\langle\eta(\mathbf{r},t)\eta(\mathbf{r}',t')\rangle=-2Mk_BT\nabla^2\delta(\mathbf{r}-\mathbf{r}')\delta(t-t')\ . \qquad (2)$$

In the above equation k_B is the Boltzmann constant and T is the temperature. Equation (2) ensures, via the fluctuation-dissipation theorem, that the stationary solution of Eq. (1) is distributed according to the Boltzmann distribution at a temperature T. After suitable rescaling of distance, time, and concentration field [20], the resulting equation of motion is

$$\frac{\partial\psi(\mathbf{r},t)}{\partial t}=\tfrac{1}{2}\nabla^2[-\psi+\psi^3-\nabla^2\psi]+\sqrt{\epsilon}\xi\ , \qquad (3)$$

where the rescaled noise term now obeys

$$\langle\zeta(\mathbf{r},t)\zeta(\mathbf{r}',t')\rangle=-\nabla^2\delta(\mathbf{r}-\mathbf{r}')\delta(t-t') \qquad (4)$$

and ϵ is the strength of the noise term.

A detailed numerical study of the preceding equation is very demanding in terms of computer time and memory, even for two-dimensional systems. First, the system has to evolve long enough time in order to reach the scaling regime. On the other hand, as time increases, the number of droplets decreases. Since we are interested in the scaling behavior of the droplet-distribution function at late times, we need to consider a very large system in order for the system to have a reasonable number of droplets at the late stages so that finite-size effects can be avoided and the results are statistically meaningful. Since the available computer time gets limited very quickly if one considers the above conditions, we are forced to make some more approximations. As a result we have not included the noise term in our studies. We note that at low temperatures, the noise term does not seem to affect some important features of the late stages of evolution (such as the growth law for the characteristic domain size and the scaling functions) for critical quenches [11]. Therefore we expect that this approximation would work reasonably well for deep off-critical quenches.

It is known that numerical integration of the discretized version of Eq. (3) develops a subharmonic bifurcation-type instability for large time steps. A linear stability analysis [11] shows that this bifurcation can be avoided by choosing the time step δt and mesh size δx such that the following inequality is satisfied in two dimensions:

$$\delta t<\frac{\delta x^4}{16-2\delta x^2}\ . \qquad (5)$$

This simple criterion turns out to be a necessary but not a sufficient condition for the stability of the numerical integration. Usually the integration is carried out by using a first-order Euler scheme. In this paper we use a more accurate method in the numerical integration of Eq. (3), namely, we use the Heun method [21], which in the absence of the noise term is a second-order Runge-Kutta scheme. We have chosen a mesh size $\delta x=1.0$ for the Laplacian discretization on a square lattice of size 540^2 for area fraction $\phi=0.05$ and 256^2 for $\phi=0.21$. With this choice for δx we have found that droplets are circular in shape, that the radius of gyration R_G of a given droplet is proportional to the geometrical radius, and that the mass of the droplet (total number of particles of the minority phase in it) is given by $2\pi R_G^2$ to a great accuracy (better than 1%). On the other hand, larger choices for δx produce anisotropic growth of droplets that reflects the underlying symmetry of the square lattice used in the numerical discretization. In Fig. 1 we show a typical morphology of the system at $t=20\,000$ for $\phi=0.21$. Note that the droplets are circular in shape as indicated by drawing circles with radii equal to $\sqrt{2}R_G$, where R_G are the corresponding radii of gyration of the clusters. Similar circular droplets are seen for $\phi=0.05$.

As mentioned above, we have considered two area fractions in our study: $\phi=0.05$ and $\phi=0.21$. One needs to be careful with the initial condition, particularly for the smaller area fraction considered. Since the system is in the metastable region of the phase diagram, a strong fluctuation is needed in the initial distribution of the order parameter in order to allow for the growth of the initial random nuclei. This is even more important in the absence of thermal noise, the case considered here. We chose the initial configuration to be a Gaussian distribution centered at $\psi_0=0.9$ with variance of magnitude 5. For this particular choice of the initial configuration the magnitude of the order parameter is very large initially at random points on the lattice and one needs a very small time step for the stability of the numerical integration in the initial stage. However, the order parameter settles down to (absolute) values smaller than unity very soon and the time step can be increased safely. We have carried out the numerical integration up to $t=20\,000$ [in the dimensionless units of Eq. (3)]. From $t=0$ to $t=100$ the

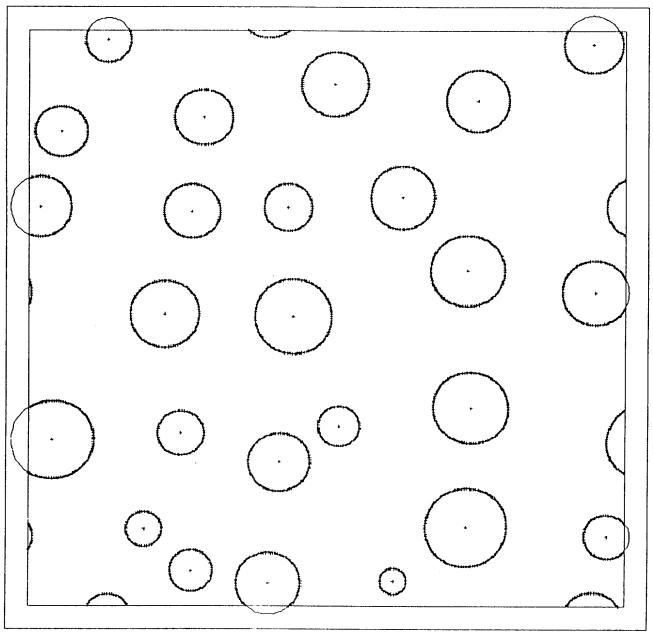

FIG. 1. A typical configuration at $t=20\,000$ during the evolution of the system for $\phi=0.21$. Note that the droplets are circular in shape as indicated by drawing circles with radii equal $\sqrt{2}R_G$, where R_G are the corresponding radii of gyration of the clusters. The parts of the circles outside the inner frame indicate images from the periodic boundary conditions.

time step is chosen to be $\delta t=0.001$, from $t=100$ to $t=1000$ the time step is $\delta t=0.025$, and for $t>1000$ δt is fixed at 0.05. In order to average over the initial random configurations, we have performed 60 runs with different initial conditions. The same parameters have been used for the case of area fraction $\phi=0.21$ except that the Gaussian distribution for the initial field is centered at $\psi_0=0.58$, since $\psi_0=1-2\phi$.

The structure formation in the system during the phase-separation process is measured by the time-dependent structure factor $S(\mathbf{k},t)$. We define the structure factor to be

$$S(\mathbf{k},t)=\left\langle \frac{1}{N}\sum_{\mathbf{r}}\sum_{\mathbf{r}'} e^{-i\mathbf{k}\cdot\mathbf{r}}[\psi(\mathbf{r}'+\mathbf{r},t)\psi(\mathbf{r}',t)-\langle\psi\rangle^2]\right\rangle , \tag{6}$$

where both sums run over the lattice of linear size L and $N=L^2$ is the total number of points in the lattice. We expect the evolution process to be isotropic and compute the circularly averaged structure factor $S(k,t)$.

We also compute the pair-correlation function defined by

$$G(\mathbf{r},t)=\sum_{\mathbf{k}} e^{i\mathbf{k}\cdot\mathbf{r}}S(\mathbf{k},t) . \tag{7}$$

Similar to the circularly averaged structure factor, we also consider a circularly averaged pair-correlation function $G(r,t)$. The correlation function is finally normalized so that its magnitude is unity at $r=0$, i.e., we define a normalized correlation function

$$g(r,t)=G(r,t)/G(0,t) , \tag{8}$$

or equivalently

$$g(r,t)=\frac{G(r,t)}{\langle\psi^2(t)\rangle-\langle\psi\rangle^2} . \tag{9}$$

A similar normalization is used for the circularly averaged structure factor $S(k,t)$. By noting that

$$\sum_{\mathbf{k}} S(\mathbf{k},t)=\langle\psi^2(t)\rangle-\langle\psi\rangle^2=G(0,t) , \tag{10}$$

we define a normalized structure factor $s(k,t)$ as

$$s(k,t)=S(k,t)/G(0,t) . \tag{11}$$

The above normalization procedure allows us to make a more reasonable comparison of the shape of the scaling functions for different area fractions, since the magnitude is normalized even though $\langle\psi\rangle$ is different for different area fractions.

Usually the location of the structure factor's maximum, k_m, is used experimentally as a measure of the characteristic domain size at some time t. However, the discrete nature of the lattice in numerical studies makes it difficult to determine k_m precisely. Previous work demonstrates that $R_g(t)$, the location of the first zero of the real-space correlation function, is a good measure for the average domain size. This length is computed by fitting a cubic polynomial to the four points closest to the first sign change in $g(r,t)$ and finding the polynomial's root. Another reliable measure of the characteristic length is the average radius of gyration $R_G(t)$ of the droplets since the droplets are found to be circular in the simulation.

III. SCALING FUNCTIONS

It is well established now that the late stages of the phase-separation process can be described in terms of scaling with a time-dependent length. The fundamental assumption of scaling is that, in the late stages of the evolution process, only one length, $R(t)$, is relevant. This characteristic length represents a measure of the typical domain size and increases with time. A main feature emerging from this picture is that the pair-correlation function $g(r,t)$ and the structure factor $s(k,t)$ depend on time through $R(t)$ only, namely,

$$g(r,t)=\mathcal{G}(r/R(t)) \tag{12}$$

and

$$s(k,t)=R(t)^d\mathcal{F}(kR(t)) , \tag{13}$$

where d is the dimensionality of the system and the functions $\mathcal{G}(\rho)$ and $\mathcal{F}(x)$ are the time-independent scaling functions of the system.

We first study the scaling behavior of the circularly averaged pair-correlation function for different area fractions. Figure 2 shows the scaling behavior of the normalized correlation function $g(r,t)$ with $R_g(t)$ as the scaling length for $\phi=0.21$. The scaling hypothesis seems to be well satisfied for $t>4000$. The corresponding scaling function for $\phi=0.05$ is shown in Fig. 3. Here also we

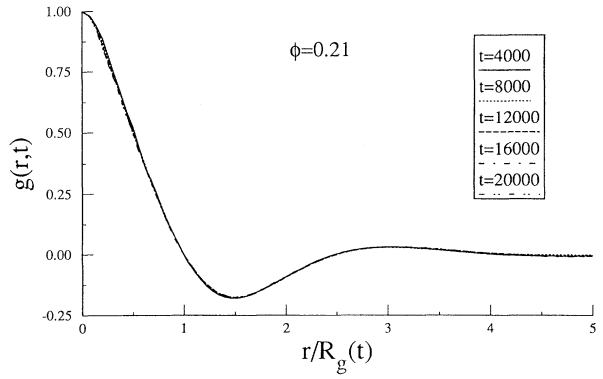

FIG. 2. Plot of the normalized pair-correlation function $g(r,t)$ vs $r/R_g(t)$ to check the scaling ansatz [Eq. (12), see text] for $\phi=0.21$.

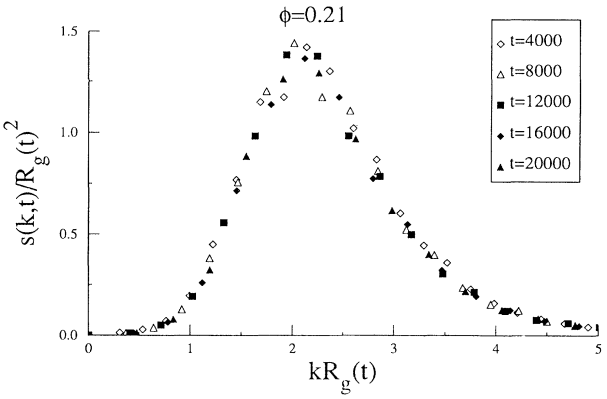

FIG. 4. Scaling plot for the normalized structure factor $s(k,t)$ with $R_g(t)$ as the scaling length for $\phi=0.21$.

find that dynamical scaling is obeyed at late times, although one finds that the scaling function obtained in this case is quite different from the one obtained in Fig. 2 for $\phi=0.21$. We will discuss this point below.

Next, we test the dynamical scaling hypothesis [Eq. (13)] for the circularly averaged and normalized structure factor $s(k,t)$ for $\phi=0.21$. In Fig. 4 we use $R_g(t)$ as the scaling length. Within the accuracy of the data scaling is well satisfied after $t=4000$ in this case. The corresponding scaling function for $\phi=0.05$ is shown in Fig. 5 now using $R_G(t)$ as the scaling length. Here also, dynamical scaling is found to be obeyed at late times ($t>8000$). Since lattice discretization does not leave us with many points for small wave vectors, the quality of the scaling is not as good for very small values of the scaling variable x.

As mentioned earlier, an important question in the study of phase separation processes is the effect of varying the volume or area fraction ϕ of the minority constituent of the binary mixture on the scaling functions. Several analytical studies have been carried out to obtain the volume fraction dependence of the scaling functions for the structure factor [22–27]. In one approach, various attempts have been made to incorporate effects of correlations among droplets in the Lifshitz-Slyozov mean-field theory which is valid in the limit of infinitesimally small volume fraction. These calculations show that the scaling functions depend on volume fractions, although the growth-law exponent does not change. Among these calculations, the theory of Tokuyama, Enomoto, and Kawasaki [22] considers both initial thermal fluctuations and nonthermal fluctuations generated by soft collisions among droplets. This theory predicts a strong dependence of the shape of the scaling functions for the structure factor on the volume fraction ϕ in three dimensions. The theory, however, is applicable only in the limit of small volume fraction ϕ (typically $\phi<10\%$) and unfortunately cannot be extended for the case of larger volume fractions due to the perturbative nature of the calculations.

Mazenko [28,29] has taken a different approach. In this theory, the order-parameter field is separated into the sum of an ordering field and a fluctuation field. When the coupling between these two fields is taken into proper account the classical LS growth law is recovered. For off-critical quenches in three dimensions [29], the above theory predicts that the scaling function computed from the pair-correlation function is an insensitive function of the volume fraction for near-critical concentration. For such concentrations, the scaling functions show a damped oscillatory behavior. However, for intermediate values of the volume fraction, the oscillatory behavior of the pair-correlation function is suppressed as the interactions between the droplets become effectively screened.

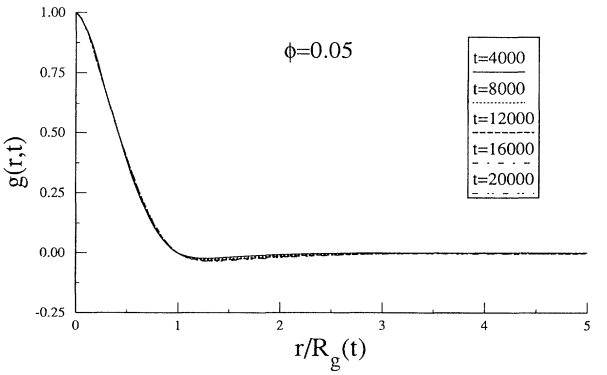

FIG. 3. Same as in Fig. 2 except $\phi=0.05$.

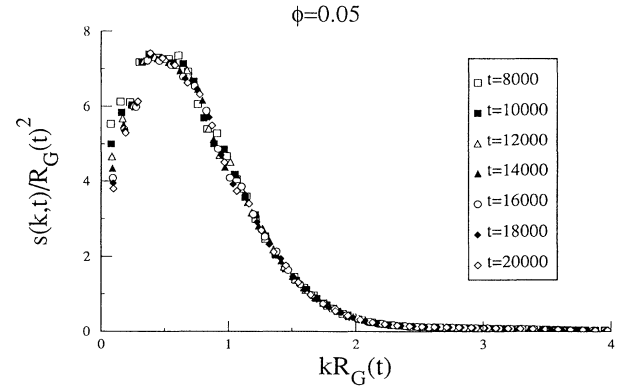

FIG. 5. Same as in Fig. 4 except $R_G(t)$ is the scaling length and $\phi=0.05$.

Very near the coexistence curve, the scaling function regains an oscillatory form but the intensity of scattering is sharply decreased.

We now compare the numerical results for the scaling functions for both the pair-correlation function and the structure factor with various theoretical predictions. The comparison with the theory of Mazenko and Tokuyama, Enomoto, and Kawasaki will be qualitative since the above theoretical calculations are valid in three dimensions. On the other hand, the explicit expressions given by a semiempirical model calculation of Fratzl and coworkers [27,30,31] permits a more detailed comparison, which we carry out later in the paper.

Let us first present the results for the scaling functions computed from the pair-correlation function. The scaling function obtained in Figs. 2 and 3 are shown in Fig. 6 along with the scaling function obtained for the critical quench by Gawlinski, Viñals, and Gunton [12]. When we compare the scaling functions for the critical quench ($\phi=0.50$) with that for $\phi=0.21$ we find that despite the radical difference in morphology (an interconnected structure for the critical quench versus droplet morphology for this off-critical case) the scaling functions are quite similar. It is, however, difficult to conclude on the basis of numerical results whether the scaling functions are actually *independent* of the area fraction in this range since numerical accuracy in $g(r)$ is lost quickly for large values of r. We should also note that the scaling functions for the pair-correlation function are not accurately known for very small values of r/R_g, since the quantity $\langle \psi^2(t) \rangle$, used in the normalization of the correlation function [see Eq. (9)], is slowly changing with time even at the very late times. This might explain the observation that the correlation function for small values of the scaling variable is not strictly linear, a form expected if Porod's law [32] is satisfied for the structure factor for large values of the wave vector. Even with these limitations on the numerically obtained correlation functions, it is still possible to realize that the scaling function for $\phi=0.05$ is *distinctly different* from that of either $\phi=0.21$ or $\phi=0.50$. The interesting feature of the scaling function for $\phi=0.05$ is that the oscillations seen in the scaling function for larger volume fractions are almost absent here and the magnitude of the pair-correlation function is very small for $r>R_g$. This suggests that the spatial correlations among the droplets are much weaker in this case. These results support the theoretical predictions of Mazenko. Although Mazenko's results are valid in three dimensions it is reasonable to expect that this theory would also yield similar qualitative results in two dimensions.

Let us now compare the qualitative features of the scaling functions for the structure factor computed here with those found in the theoretical calculations of Tokuyama, Enomoto, and Kawasaki for three-dimensional systems. In Figs. 7 and 8 we plot the scaling functions for the *unnormalized* structure factors for different values of ϕ and with $R_g(t)$ and $R_G(t)$ as the corresponding scaling lengths. Note that for $\phi=0.50$ only $R_g(t)$ is used as the scaling length since in this case the domain morphology is interconnected and one cannot define a droplet radius of gyration. Comparing these unnormalized scaling functions for various area fractions, one finds that the scaling function depends strongly on the area fraction and the scattering intensity, as given by the maximum value of the structure factor, decreases monotonically with the area fraction. These features are in good qualitative agreement with the above theory. In order to compare the shapes of the scaling functions, however, one should use the normalized structure factor $s(k,t)$ defined above. In Figs. 9 and 10 we plot the normalized scaling functions for various area fractions with $R_g(t)$ and $R_G(t)$ as the corresponding scaling lengths. Comparing the scaling functions for $\phi=0.05$ and $\phi=0.21$ in Fig. 9, we find that as the area fraction is decreased, the half widths of the scaling functions increase, the location of the peak of the scaling function shifts towards smaller reduced wave vectors and the peak height decreases. In Fig. 10 also, we find similar qualitative features [33] when we compare the scaling functions for $\pi=0.05$ and $\phi=0.21$. However, when we compare the normalized scaling functions for $\phi=0.21$ and $\phi=0.50$ in Fig. 9, we find that despite the different morphologies of the domain structure, the scaling functions are very similar. Both scaling functions

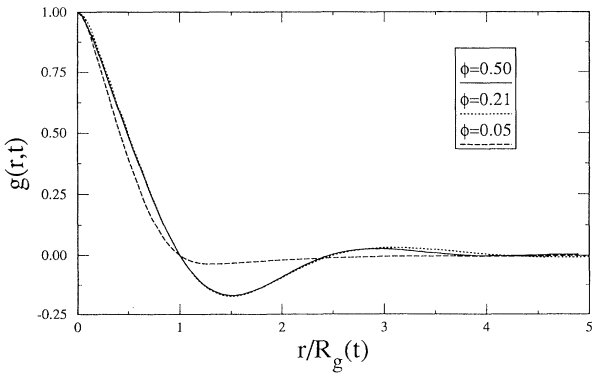

FIG. 6. Comparison of the scaling function obtained from the pair-correlation function for various values of the area fraction ϕ. The result for $\phi=0.50$ is taken from Ref. [12]. Note that the scaling function is very similar for $\phi=0.50$ and $\phi=0.21$ whereas it differs significantly from the above ones for $\phi=0.05$.

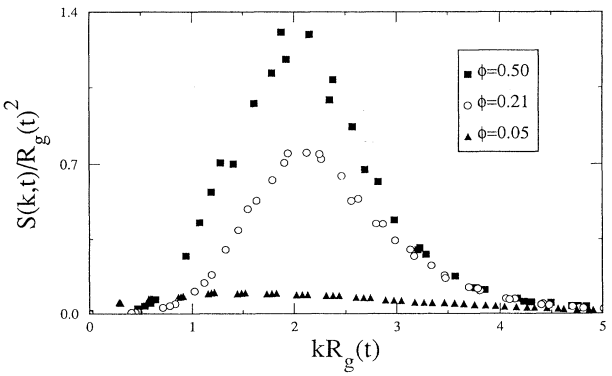

FIG. 7. Comparison of the scaling function obtained from the *unnormalized* structure factor $S(k,t)$ with $R_g(t)$ as the scaling length for various values of the area fraction.

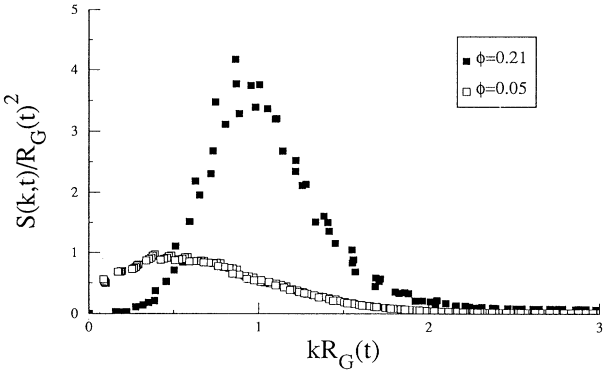

FIG. 8. Same as in Fig. 7 except $R_G(t)$ is the scaling length.

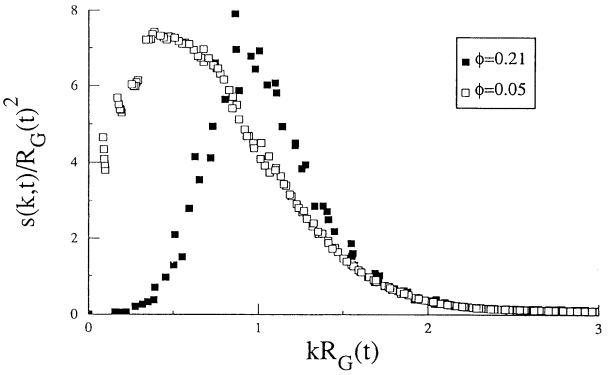

FIG. 10. Same as in Fig. 9 except $R_G(t)$ is the scaling length.

have a similar shape and the peak is located at almost the same position. It is difficult again to assert whether the scaling function is strictly independent of the area fraction at this range but it is apparent that the change in the two scaling functions is very small given the fact that the area fraction changes by a factor of about 2.5 between the two cases. Since the theory of Tokuyama, Enomoto, and Kawasaki breaks down for these large volume fractions it is not possible to compare the qualitative features with that theory. As mentioned earlier, Mazenko's theory agrees well with our general findings for the pair-correlation function.

Fratzl and Lebowitz [30] have proposed a semiempirical model expression for the scaling functions based on a mathematical model and some general features of the structure function [27], in particular the fact that the structure function $s(k,t)$ for small value of the wave vector k should be proportional to k^4 [34,35]. The approach of Fratzl and Lebowitz allows an explicit expression for the scaling functions and it has been rather successful in describing data coming from computer simulations [27–30] or experimental data on binary alloys [31]. The scaling functions are constructed in two stages: (1) The pair-correlation scaling function is, in principle, modeled by an oscillatory decreasing function

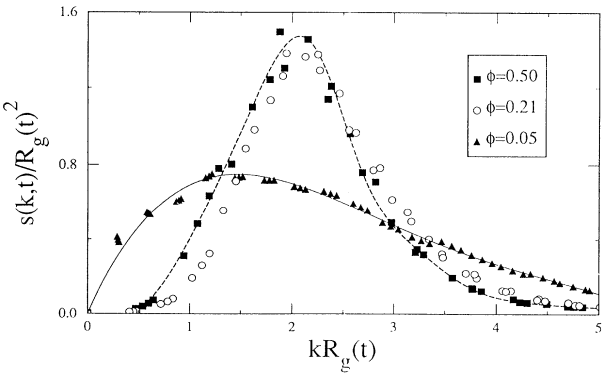

FIG. 9. Comparison of the scaling function obtained from the *normalized* structure factor $s(k,t)$ with $R_g(t)$ as the scaling length for various values of the area fraction. The solid and the dotted lines are guides to the eye for $\phi=0.05$ and 0.50, respectively.

$$e^{-\lambda\rho}\frac{\sin(2\pi\rho/\Delta)}{2\pi\rho/\Delta}\ , \tag{14}$$

where λ is a constant proportional to the amount of the total interface present per unit area and Δ is another constant related to the typical domain size. (2) The second stage consists of incorporating the small-k behavior mentioned above by multiplying the Fourier transform of the above expression by the function $a_2x^4/(x^4+c_2)$, a_2 and c_2 being two constants. The final expression for the scaling function $\mathcal{F}(x)$ is then (in two dimensions)

$$\mathcal{F}(x)=\frac{a_2x^4}{x^4+c_2}\{(3+y^2)[y+(3+y^2)^{1/2})]\}^{-1/2}\ , \tag{15}$$

where

$$y=\frac{x^2-1}{b_2}-1+d_2 \tag{16}$$

and d_2 and b_2 are constants depending on λ and Δ. The corresponding pair-correlation scaling function is obtained by the inverse two-dimensional Fourier transform of the above expression, namely,

$$\begin{aligned}\mathcal{G}(\rho)&=\int d\mathbf{x}\,e^{-i\mathbf{x}\cdot\rho}\mathcal{F}(x)\\&=2\pi\int_0^\infty dx\,xJ_0(x\rho)\mathcal{F}(x)\ ,\end{aligned} \tag{17}$$

where $J_0(z)$ is the zeroth-order Bessel function.

When comparing the scaling functions $\mathcal{F}(x)$ and $\mathcal{G}(\rho)$ with Eqs. (15) and (17), respectively, one has to consider the fact that the axes have to be rescaled in order to take into account that the scaling lengths might be different. The easiest way to achieve this is to rescale the axes for the function $\mathcal{F}(x)$ in such a way that this function has its maximum located at $x_{\max}=1$ and the value of the function is unity there, i.e., $\mathcal{F}(x_{\max})=1$. In theoretical expression Eq. (15) the above two requirements fix two of the parameters, for instance, a_2 and c_2, in terms of the other two, b_2 and d_2. This leaves us with two free parameters to fit the data. The fitting is not free of problems, though, because, as mentioned above, it is difficult to accurately determine the maximum of the numerically determined scaling function $\mathcal{F}(x)$. Once this axes rescaling has been performed, a least-squares fitting of expression (15) to the simulation data yields the following

values for the parameters: $b_2=0.391$, $d_2=0.644$ for $\phi=0.50$; $b_2=0.383$, $d_2=0.932$ for $\phi=0.21$; and $b_2=2.196$, $d_2=0.528$ for $\phi=0.05$ (in this latter case of $\phi=0.05$ only values satisfying $x \geq 1$ have been included in the fit). Following Fratzl and Lebowitz, and considering that the value for d_2 is not very critical for the fit, we can also fix the value of d_2 to be a constant ($d_2=0.6$) independent of the area fraction, and consider b_2 to be the only adjustable parameter. A least-squares fit in this case yields $b_2=0.387, 0.371, 2.377$ for $\phi=0.50, 0.21, 0.05$, respectively. These values again confirm that the variation between the scaling functions for $\phi=0.50$ and $\phi=0.21$ is very small. The fact that the scaling function does not vary much between $\phi=0.5$ and $\phi=0.21$ but then broadens strongly for small ϕ is in good agreement with general considerations about the surface-to-volume ratio in these two-phase systems [27,30,31]. Indeed, one finds in Fig. 2 of Ref. [31] that the width of the scaling function (normalized so that the maximum is located at $x=1$) hardly changes between $\phi=0.5$ and $\phi=0.2$. It starts to increase strongly only below $\phi \approx 0.1$. Although this figure in Ref. [31] is for the three-dimensional case, a similar qualitative behavior is expected in two dimensions.

Figures 11–13 compare the scaling function $\mathcal{F}(x)$ with rescaled axes with the theoretical prediction for the different values of the parameters mentioned above. The general agreement is rather good except, perhaps, for intermediate values of the scaling variables where the theoretical prediction is systematically larger than the simulation data and, in the case of $\phi=0.05$, also for small values of the scaling variable x. Figures 14–16 show the comparison of Eq. (17) for the scaling function $\mathcal{G}(\rho)$ using the same parameters obtained above and after a rescaling of the axes in such a way that $\mathcal{G}(0)=1$ and $\mathcal{G}(1)=0$. As mentioned above, the scaling functions for the pair-

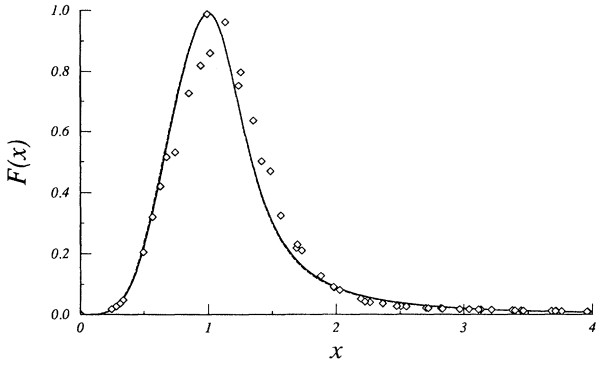

FIG. 11. Comparison of the scaling function with the semiempirical model calculation of Fratzl and co-workers [27,30,31]. Here we compare the scaling function for the structure factor obtained for $\phi=0.50$. The solid line is the fit treating both b_2 and d_2 as free parameters [see Eqs. (15) and (16); the other two constants are obtained by rescaling the location of the maximum and the peak of the structure function; see text] and the best fit corresponds to $b_2=0.391$ and $d_2=0.644$. The dashed line is the best fit when d_2 is kept fixed at 0.6. The corresponding value of b_2 is 0.387.

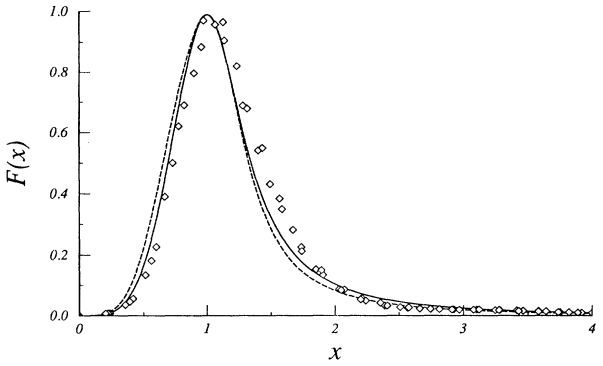

FIG. 12. Same as in Fig. 11 except for $\phi=0.21$. The solid line is the fit treating both b_2 and d_2 as free parameters, yielding $b_2=0.383$ and $d_2=0.932$. The dashed line is the best fit when d_2 is kept fixed at 0.6. The corresponding value of b_2 is 0.371. Note that the value of b_2 in each case is very similar to the ones obtained for $\phi=0.50$.

correlation function is not accurately known for very small values of ρ, since the quantity $\langle \psi^2(t) \rangle$ is slowly changing with time. One could then possibly improve these fits of $\mathcal{G}(\rho)$ slightly by using a different rescaling for the vertical axis, but we have preferred to maintain the condition $\mathcal{G}(0)=1$.

In Figs. 17 and 18 we show the scaling functions for the normalized structure factors in log-log plots. It is easy to determine the small and large (reduced) wave-vector behavior of the scaling function if plotted in this fashion. Several important features are evident from these figures. First of all, a secondary maxima shows up in all of the scaling functions around a wave vector k which is about twice the wave vector k_m where the major peak of the scaling function is located. This shoulder has been seen in previous numerical [36] and theoretical [37] studies of critical quenches as well as in experiments [38]. It is well known that Porod's law [32] gives the leading-order term for the structure factor for large values of k: $S(k,t) \sim k^{-3}$ in two dimensions. However, there could

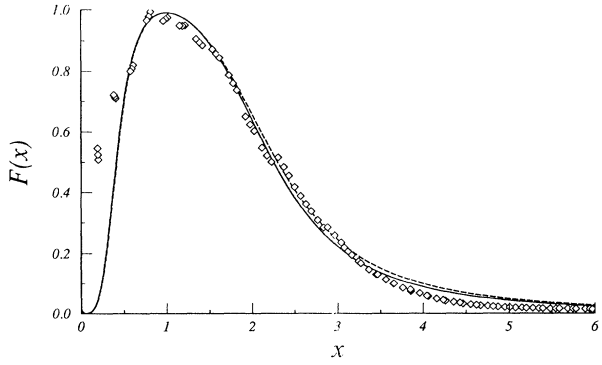

FIG. 13. Same as in Fig. 11 except for $\phi=0.05$. The solid line is the fit treating both b_2 and d_2 as free parameters, yielding $b_2=2.196$ and $d_2=0.528$. The dashed line is the best fit when d_2 is kept fixed at 0.6. The corresponding value of b_2 is 2.377. Note that the value of b_2 in this case is quite different from the ones obtained for $\phi=0.50$ and $\phi=0.21$.

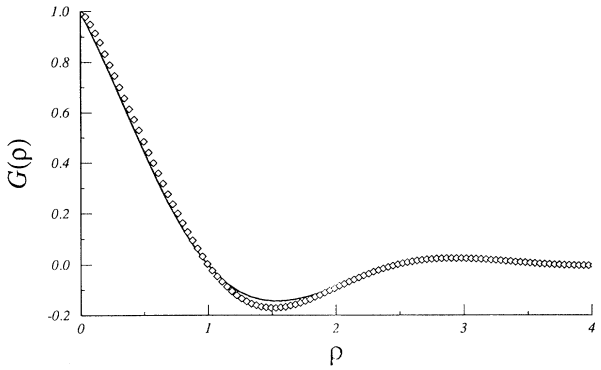

FIG. 14. Comparison of the scaling function with the semiempirical model calculation of Fratzl and co-workers [27,30,31]. Here we compare the scaling function for the pair-correlation function obtained for $\phi=0.50$. The solid line and dashed lines are obtained by using the fitting parameters in Fig. 11 and using Eq. (17).

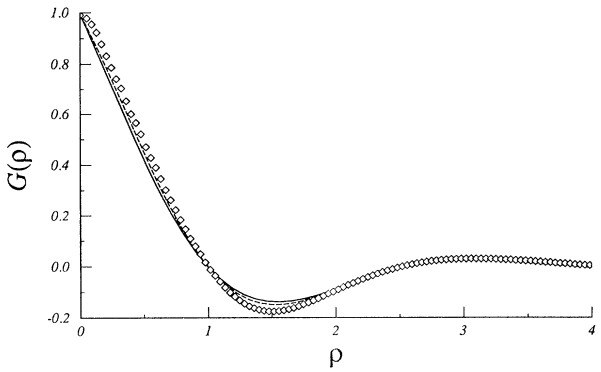

FIG. 15. Same as in Fig. 14 except for $\phi=0.21$. The solid line and dashed lines are obtained by using the fitting parameters in Fig. 12 and using Eq. (17).

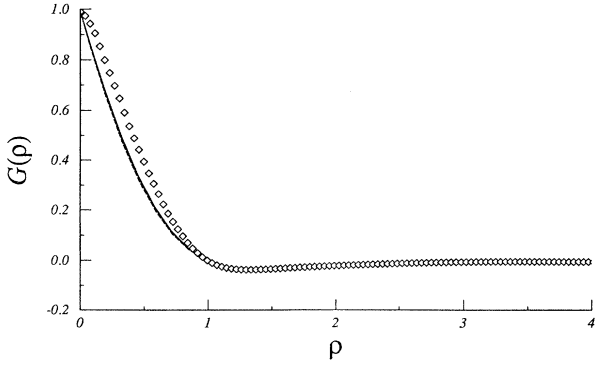

FIG. 16. Same as in Fig. 14 except for $\phi=0.05$. The solid line and dashed lines are obtained by using the fitting parameters in Fig. 13 and using Eq. (17).

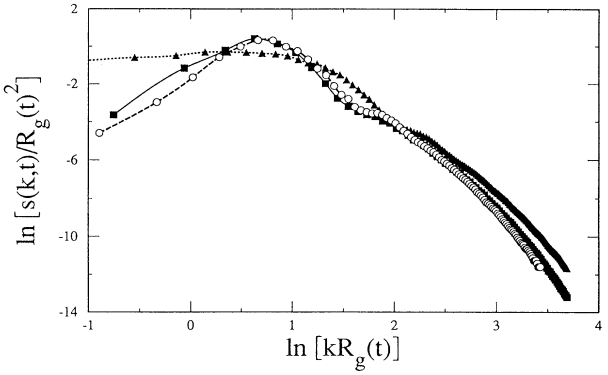

FIG. 17. Log-log plot of the scaling functions in Fig. 9. The lines are guides to the eye.

be oscillations about this leading-order term which can arise, for example, from a monodisperse distribution of spheres [39,40]. The magnitude of the oscillations depends on the width of the size distribution of these "monodisperse" regular objects [27]. We should also note here that an oscillatory behavior in the scaling function for the structure factor is also obtained in a simplified model calculation by Rikvold and Gunton [23] where the model describes the morphology of the late-time growth process in terms of a gas of spherical droplets of the minority phase, surrounded by depletion zones.

Another important feature is that although all the scaling functions are essentially parallel to each other for large k values, the functional form for $\phi=0.05$ seems to be different from the other two scaling functions for small values of k. For small k the scaling function increases approximately as k^4 for $\phi=0.21$ and $\phi=0.50$, in accordance with recent theories [34,35]. Although these theories would predict a similar k dependence for the scaling function for $\phi=0.05$ as well, we find the scaling function to be quite flat for small wave vectors. We note, however, that the scaling function contains only a few points for small values of k and we are therefore probably unable to access sufficiently small wave vectors where the theoretical results would be applicable. Since it is difficult to access small wave vectors in a numerical study due to lattice discretizations, one needs to study a much larger system to resolve this important issue. However,

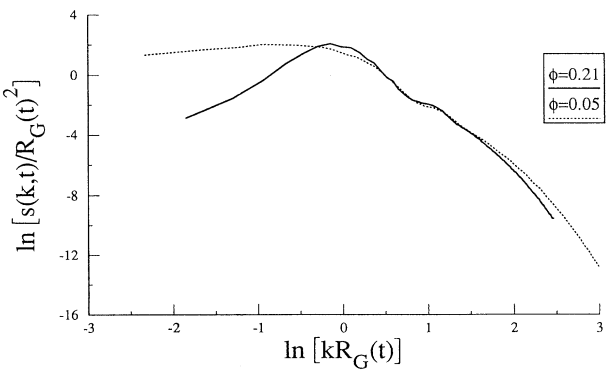

FIG. 18. Log-log plot of the scaling functions in Fig. 10.

there is no physical argument that we know of that would suggest the behavior should be different from k^4 for very small k, so we would speculate that this is indeed the behavior that one would find in studies of much larger systems.

IV. DROPLET-DISTRIBUTION FUNCTION

Many theoretical studies of the final stages of the nucleation and growth process (also known as Ostwald ripening) have been carried out for both two- and three-dimensional systems. The main feature shared by all these analytical calculations is that they involve some systematic or approximate expansion in terms of the volume fraction and are supposed to be valid only for small values of ϕ. As mentioned above, the classical Lifshitz-Slyozov theory ignores spatial interaction among droplets and thus is only valid in the limit of zero volume fraction. Many attempts have been made to systematically include the correlation among droplets in some approximate way in the theoretical calculations. It has been found that these improvements do not change the growth-law exponent but can substantially change the shape of the droplet-distribution function, depending on the assumptions made. Since we have been able to access quite small area fractions in our two-dimensional simulations where different theoretical calculations are assumed to be correct, we will compare the numerically obtained droplet-distribution functions with various approximate theories to find out their validity and applicability.

The theoretical studies predict that the droplet-distribution function should have a scaling form valid at late times. The scaling assumption is that there is only one relevant length. This can be defined, for instance, as the mean value of the radius,

$$\langle R(t)\rangle = \int_0^\infty R f_R(R,t) dR \ , \tag{18}$$

where $f_R(R,t)$ is the probability density function for the droplet radius at time t. It is then natural to define the new scaling variable $x_0 = R/\langle R(t)\rangle$. It is obvious that the mean value of x_0 is $\langle x_0\rangle = 1$. The probability density function for the variable x_0 is

$$f_{x_0}(x_0,t) = \frac{dR}{dx_0} f_R(R,t) = \langle R(t)\rangle f_R(R,t) \ . \tag{19}$$

Scaling affirms that, at late enough times, the function $f_{x_0}(x_0,t)$ is independent of time t, i.e., $f_{x_0}(x_0,t) = f_{x_0}(x_0)$.

In this numerical study we have computed, among other quantities, the probability distribution function $f_R(R,t)$, such that $f_R(R,t)\delta R$ is the probability of finding a droplet of radius between $R - \delta R/2$ and $R + \delta R/2$. Strictly speaking, we have computed the probability distribution function $f_l(l,t)$ for the droplet size l (number of particles of the minority phase belonging to the cluster). However, as mentioned above, droplets are circular in shape and the relation between two magnitudes is $l = \pi R^2$, which allows the calculation of $f_l(l,t)$ from $f_R(R,t)$ and vice versa. Even for a 540^2 lattice the number of droplets at late times is not very large (around 30–40 for the smallest area fraction $\phi = 0.05$) and the values of δR necessary to get smooth data need to be increased with time. Similarly, for $\phi = 0.21$ the number of droplets at the latest time was about 25–30 for a 256^2 lattice. In order to improve statistics we have calculated $f_R(R,t)$ by counting the number of droplets with radii between $R - \delta R/2$ and $R + \delta R/2$. The necessary values of δR to get smooth data need to be increased with time, e.g., $\delta R = 0.15, 0.25, 0.35$ for $t = 1000, 10\,000, 20\,000$ for $\phi = 0.05$ and $\delta R = 0.16, 0.20, 0.26$ for $t = 1000, 10\,000, 20\,000$ for $\phi = 0.21$.

In Figs. 19 and 20 we study the scaling for the droplet-distribution function for area fractions $\phi = 0.21$ and $\phi = 0.05$, respectively. We find that scaling is reasonably satisfied in both cases at late times, although the quality of the scaling is much better for $\phi = 0.05$. Although our data is taken from simulations in quite large systems, the numerical data has some scatter for $\phi = 0.21$ and we believe that simulations in much larger systems are necessary for definitive comparisons with theoretical predictions. This, however, seems to be beyond the reach of current supercomputers.

The various theories differ in their prediction for the scaling function $f_{x_0}(x_0)$. In order to compare with theoretical predictions, one needs to note that the scaling variable used in different theories varies from one to another. In general, the scaling variable x is defined as $x = R/R^*(t)$ where $R^*(t)$ is some time-dependent length that might or might not coincide with $\langle R(t)\rangle$. However, due to the scaling hypothesis, one can assume that $R^*(t)$ will be proportional to $\langle R(t)\rangle$, and so the scaling variable x_0 used in our study and the general scaling variable x introduced in the theory will be proportional to each other, i.e., $x_0 = x/\alpha$, with α some time-independent constant. By using the relation $\langle x_0\rangle = 1$ we can conclude that $\alpha = \langle x\rangle$ and then $x_0 = x/\langle x\rangle$. The probability density function of x, $f_x(x)$, will be related to the probability density function of x_0 by the relation

$$f_{x_0}(x_0) = \frac{dx}{dx_0} f_x(x) = \langle x\rangle f_x(x) = \langle x\rangle f_x(x_0\langle x\rangle) \ . \tag{20}$$

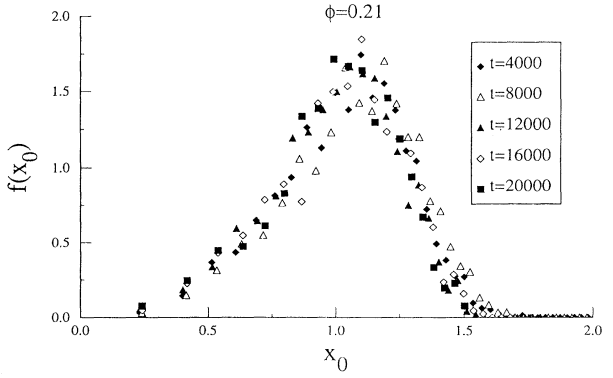

FIG. 19. Simulation data for droplet-distribution function for different times and for $\phi = 0.21$.

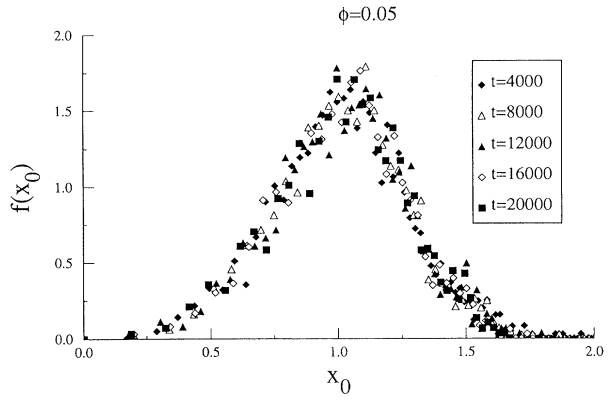

FIG. 20. Same as in Fig. 19 except for $\phi=0.05$.

This relation allows us to compare the simulation data with the theoretical predictions.

Let us now briefly review the different theoretical predictions. Rogers and Desai [16] carried out a simple extension of Lifshitz-Slyozov theory in two dimensions. However, in two dimensions, there seems to be no consistent steady-state result in the limit of $\phi\to 0$. In the non-steady-state calculation for $\phi\to 0$, Rogers and Desai found a scaling form for the droplet-distribution function which we will loosely call the "Lifshitz-Slyozov (LS)" scaling function in two dimensions. This scaling function $f_x^{\rm LS}(x)$ is given by

$$f_x^{\rm LS}(x)=\tfrac{8}{27}x^2\left[1-\frac{2x}{3}\right]^{-28/9}\left[1+\frac{x}{3}\right]^{-17/9}\times\exp\left[\frac{-4x}{9-6x}\right]. \tag{21}$$

This distribution is cut off for values of $x\geq 1.5$. For this distribution one obtains $\langle x\rangle=1.0665$. We should also note here that for this non-steady-state calculation in the limit $\phi\to 0$, Rogers and Desai found that the average droplet radius $\langle R(t)\rangle$ grows as $\langle R(t)\rangle\sim(t/\ln t)^{1/3}$.

The next theoretical prediction we consider is that of Ardell [41]. The author has recently extended his earlier theory [42] for two-dimensional systems. This theory includes the effect of diffusive correlations among nearest-neighbor clusters by introducing an *ad hoc* cutoff limit in the diffusion geometry. In the limit of $\phi\to 0$, Ardell [41] also finds the same scaling form [Eq. (21)] as obtained by Rogers and Desai in two dimensions. The distribution function needs to be evaluated numerically for each finite area fraction in the following way. In Ardell's theory the expression for the scaling function $f_x^A(x)$ is

$$f_x^A(x)=g(x)\exp\left[-\int_0^x g(u)du\right], \tag{22}$$

where the function $g(x)$ is given by

$$g(x)=\frac{-2x^2}{\dfrac{(x-1)\xi}{\ln\left[1+\dfrac{1}{\eta x}\right]}-x^3}. \tag{23}$$

The parameter η is related to the area fraction ϕ by

$$\eta=\frac{4\phi^{1/2}}{e^{4\phi}\Gamma(\frac{1}{2},4\phi)} \tag{24}$$

and $\Gamma(x,y)$ is the incomplete gamma function [43]. This distribution is cut off for values $x\geq x_m$, where x_m is given by the solution of the equation

$$(1+\eta x_m)\ln\left[1+\frac{1}{\eta x_m}\right]=\frac{x_m-1}{2x_m-3} \tag{25}$$

and

$$\xi=\frac{x_m^3}{(2x_m-3)(1+\eta x_m)}. \tag{26}$$

In Marqusee's theory [44], the surrounding droplets are considered as an "effective medium" and the distribution function is derived in a self-consistent fashion. Again, no closed form for the distribution is found and it needs to be evaluated numerically for each area fraction. We briefly describe the numerical evaluation process below. In Marqusee's theory, the droplet distribution function $f_x^M(x)$ is given by

$$f_x^M(x)=\frac{F_0(x)}{\int_0^\infty F_0(x)dx}, \tag{27}$$

where the function $F_0(x)$ is defined as

$$F_0(x)=\frac{\text{const}}{\omega(x,\sigma_1)}\exp\int_0^x\omega^{-1}(x',\sigma_1)dx' \tag{28}$$

and the function $\omega(x,\sigma_1)$ is

$$\omega(x,\sigma_1)=\frac{3}{2}\frac{1}{\xi_0}\frac{K_1(x/\xi_0)}{K_0(x/\xi_0)}[\sigma_1-1/x]-x/2, \tag{29}$$

where $K_0(z)$ and $K_1(z)$ are modified Bessel functions [43] and the constant in Eq. (28) is determined by the normalization condition

$$\int_0^\infty x^2F_0(x)dx=1. \tag{30}$$

The distribution is cut off for values of $x\geq x_0$ where x_0 and the parameter σ_1 are obtained as the solution of the next two equations:

$$w(x,\sigma_1)_{x=x_0}=0, \tag{31}$$

$$\frac{d}{dx}\omega(x,\sigma_1)_{x=x_0}=0. \tag{32}$$

Finally, the parameter ξ_0 has to satisfy the consistency relation

$$\xi_0^{-1}=2\phi\int_0^\infty x\frac{K_1(x/\xi_0)}{K_0(x/\xi_0)}F_0(x)dx. \tag{33}$$

Marqusee's theory has recently been extended and generalized by Zheng and Gunton [45]. They use a new expansion parameter (instead of $\phi^{1/2}$ used by Marqusse) and show that there is no finite cutoff for the scaled distribution function. However, the authors expect that this scheme breaks down for $\phi>0.01$. Marsh and Glicksman

[46] have also developed a theory of two-dimensional coarsening of collections of flat disks. This theory is an extension of the mean-field approach of the authors in three dimensions [47]. In this theory, the statistical correlation between particles is determined through global constraints over the size distribution.

Recently, Yao *et al.* [48] have used a mean-field approach for both two- and three-dimensional systems. In their theory, many droplet correlation effects are approximated in the same manner as the Thomas-Fermi approach for a Coulombic system. In this mean-field calculation it is assumed that the growth rate for each droplet is only proportional to the difference between the boundary concentration and the average bulk concentration. Also, an equation of motion for the local concentration field is written in an approximate form such that local diffusion is modified by the effective diffusion field from other droplets, giving rise to a screening length ξ. Finally, the curvature-dependent rate coefficient for the growth law is determined self-consistently. However, this theory is inapplicable when the screening length is close to the average radius of droplets and the authors found that the calculations break down for $\phi > 0.085$ in two dimensions. These authors also find that there is no consistent steady-state limit in two dimensions, as manifested in a logarithmic singularity in the growth-law rate for $\phi \to 0$. In this limit, however, the authors are able to calculate the droplet-distribution function reproducing the result [Eq. (21)] found by Rogers and Desai [16] and also by Ardell [41].

In Figs. 21 and 22 we compare the predictions of different theories with the numerical data for area fractions $\phi = 0.21$ and $\phi = 0.05$, respectively. For an easier comparison with different theories, we show the result for the distribution functions only for the latest time ($t = 20\,000$) in the above figures. In the above figures we do not show the results of Zheng and Gunton or of Marsh and Glicksman, since these distribution functions differ significantly from the simulation results. For example, the calculations of Zheng and Gunton yield a distribution function that is much too short near the peak (for $\phi = 0.05$ the maximum height of the Zheng and Gunton

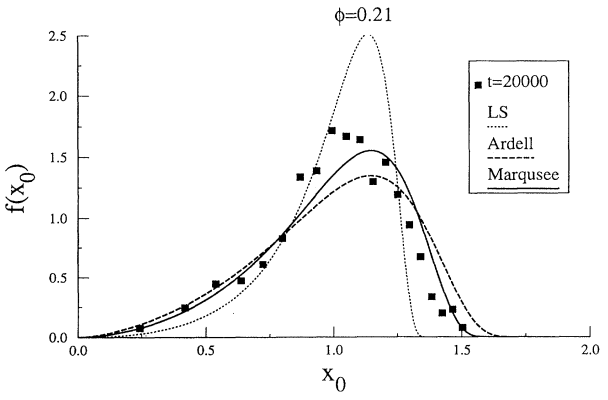

FIG. 21. Simulation data for droplet-distribution function at the latest time ($t = 20\,000$) for $\phi = 0.21$ compared with various theories.

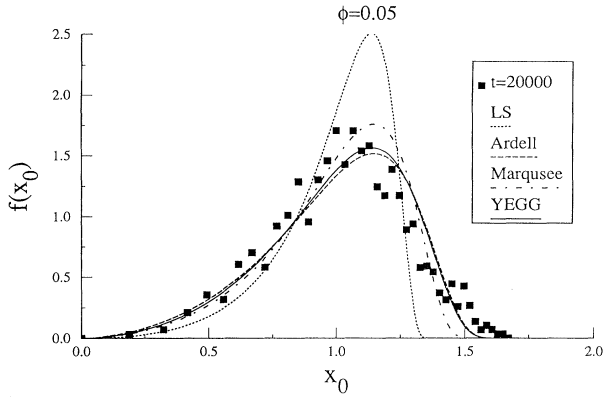

FIG. 22. Same as in Fig. 21 except for $\phi = 0.05$.

distribution function is about 1.0). It seems that this theory does not work well for these area fractions. In this context we note here that the above authors themselves also acknowledge the fact that their approximations are likely to break down when $\phi \approx 0.01$.

From both Figs. 21 and 22 we find that the LS scaling function is sharper and much higher in the peak than the corresponding numerical data. These discrepancies are expected since, as mentioned earlier, the LS results are only valid in the limit of zero volume fraction. For $\phi = 0.05$ we find that the data agree reasonably well (Fig. 22) with the predictions of Yao *et al.* (YEGG) and Ardell (actually, the difference between these two theories is very small except near the peak). We note that there are small differences between the theoretical predictions and the numerical data both near the peak and the tail of the distribution. It seems that the location of the maximum is slightly different in the numerical distribution function. Since the uncertainties in the numerical results are larger near the tail of the distribution, it is difficult to judge whether the discrepancy near the tail is real or not. For $\phi = 0.21$, the theory of Yao *et al.* breaks down and does not yield any result. Ardell's result also does not compare well with the simulation data (Fig. 21). It seems that, for this area fraction, Marquesee's theoretical result comes close to the simulation results. However, there appears to be some systematic differences between the data and the theory. It seems then that a complete theoretical description of the late-stage growth process in two dimensions is still incomplete, and we hope that our numerical work would direct attention to this direction.

V. GROWTH LAW

At sufficiently late times, the characteristic length scale $R(t)$ [given by any of the measures $R_g(t)$ or $R_G(t)$] is expected to grow as t^n. The classical theory of Lifshitz and Slyozov, valid only in the limit where the volume fraction occupied by droplets goes to zero, i.e., near the coexistence curve in the nucleation regime, predicts $n = \frac{1}{3}$ in three dimensions. As mentioned above, Yao *et al.* find that there is no consistent steady-state limit in two dimensions, as there is a logarithmic singularity in the growth-law rate for $\phi \to 0$. However, for small but finite

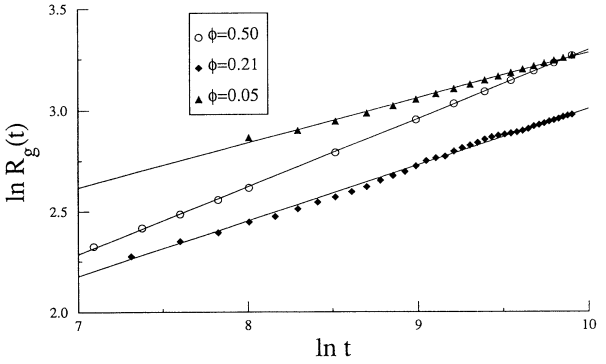

FIG. 23. Log-log plot of the characteristic domain size $R_g(t)$ vs time t for various area fractions ϕ. The solid lines are best fit to the data. The result for $\phi=0.50$ is taken from Ref. [12].

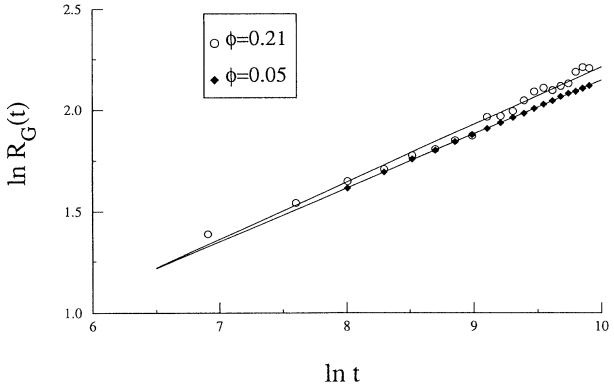

FIG. 25. Same as in Fig. 23 except $R_G(t)$ is the characteristic length.

area fractions these authors find that the asymptotic growth law for the characteristic domain size can be written as $R^3(t)=A+Bt$, where A and B are constants. In the limit of $t\to\infty$ this growth law can be written in an equivalent form: $R(t)\sim t^{1/3}$. It is also interesting to note here again that for the non-steady-state calculation in the limit $\phi\to 0$, Rogers and Desai found that the average droplet radius $\langle R(t)\rangle$ grows as $\langle R(t)\rangle\sim(t/\ln t)^{1/3}$.

The Lifshitz-Slyozov theory, based on a mechanism of evolution governed by bulk diffusion across the interfaces, has been qualitatively extended by Huse [8] to the case of equal volume fraction of the two phases. Since then, it has been well established in the literature both by analytical calculations [9] and by large-scale computer simulations [10–12,49] that the asymptotic growth-law exponent is $\frac{1}{3}$ even for critical quenches. Thus the growth exponent remains the same when the volume fraction (or the area fraction) is changed from a small value to the critical concentration. In this study we would like to confirm these predictions for various area fractions. Moreover, our objective is to find out how the *magnitude* of the characteristic domain size varies with the area fraction as well.

In Fig. 23 we show a log-log plot for the measure of the domain size $R_g(t)$ vs time for three different area fractions. Again, the results for $\phi=0.50$ are taken from Ref. [12] for comparison. This log-log plot yield an effective exponent of 0.33 ± 0.01, 0.28 ± 0.02, and 0.23 ± 0.02 for $\phi=0.50$, 0.21, and 0.05, respectively. It is interesting to note that the magnitudes of the length scale R_g are similar for $\phi=0.50$ and $\phi=0.05$ at the late times accessed in this simulation, although the effective exponent in these two cases are different. For $\phi=0.21$, however, the magnitude is smaller than the above two cases.

In Fig. 24 we plot the same data for $R_g(t)$ vs $t^{1/3}$ for three different area fractions. We find that the data can be fitted by straight lines in each case, confirming that the asymptotic growth law exponent is $\frac{1}{3}$ in all these cases.

In Fig. 25 we show a log-log plot for the other measure of the domain size considered in this study, namely, the average radius of gyration $R_G(t)$. As mentioned above, this length scale can only be defined for off-critical concentrations and thus the results are shown only for $\phi=0.21$ and $\phi=0.05$. At the latest time accessed in the simulation, we find that the magnitude of this measure is slightly larger for $\phi=0.21$ than for $\phi=0.05$. The log-log plot yields effective exponents of 0.28 ± 0.02 and 0.27 ± 0.02 for $\phi=0.21$ and 0.05, respectively. The fact that these are actually effective exponents can be realized by plotting the same data for $R_G(t)$ vs $t^{1/3}$ for the above two area fractions in Fig. 26. We find again that the data

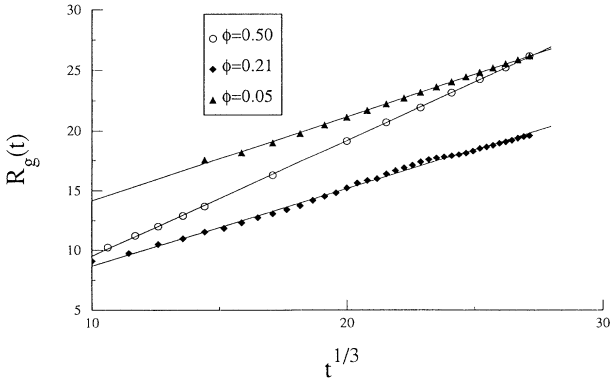

FIG. 24. The characteristic domain size $R_g(t)$ plotted against $t^{1/3}$ for various area fractions ϕ. The solid lines are best fit to the data. The result for $\phi=0.50$ is taken from Ref. [12].

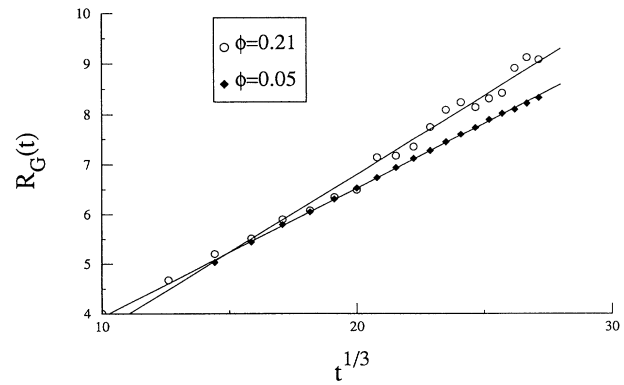

FIG. 26. Same as in Fig. 24 except $R_G(t)$ is the characteristic length.

can be fitted by straight lines in each case, confirming that the asymptotic growth law exponent is $\frac{1}{3}$.

VI. CONCLUSIONS

In this paper we have numerically studied the dynamics of the phase-separation process in the context of the Cahn-Hilliard model in two-dimensional systems. In our study we have considered various values of the area fraction of the minority component of a binary mixture and investigated the effect of this area fraction on experimentally accessible quantities such as the scaling function for the structure factors and the characteristic size of the growing domains. We have focused on the late-time behavior for reasonably large system sizes. We find that, at sufficiently late times, the scattering intensity and pair-correlation functions are well represented in terms of scaling with a time-dependent length. We have analyzed how the shape of the scaling functions obtained both from the pair-correlation function and the structure factor changes as one varies the area fraction. Whenever possible we have compared the numerical results with theoretical predictions. Since some of the theoretical predictions are valid in three dimensions, in many cases this comparison is only qualitative.

We have also considered the scaling behavior for the droplet-distribution functions and found that dynamical scaling is obeyed by this function as well. There are several theoretical predictions about the shape of the droplet-distribution function in two dimensions. We have compared the numerical results with different theoretical predictions in order to understand the validity and applicability of these approximate calculations.

Finally, we have also analyzed the growth law for the characteristic domain size for various area fractions. Our analysis of the time dependence of various measures for the characteristic length supports a modified Lifshitz-Slyozov law in which the asymptotic growth-law exponent is $\frac{1}{3}$ for all area fractions.

ACKNOWLEDGMENTS

This work was partially supported by NSF Grant No. DMR-9100245 and a grant of computer time at the Pittsburgh Supercomputing Center. Acknowledgment is also made to the Donors of the Petroleum Research Fund, administered by the American Chemical Society for partial support of this work. R.T. acknowledges financial support from the Dirección General de Investigación Científica y Técnica, Contract No. PB 89-0424 (Spain). A. C. thanks UIB for the warm hospitality while part of this work was carried out. We thank Dr. Qiang Zheng, Dr. J. Viñals, Professor Hong Guo, and Professor E. Gawlinski for providing us with their numerical results and Professor P. Fratzl and Professor J. Lebowitz for helpful comments and discussions, and a critical reading of the manuscript.

[1] J. D. Gunton, M. San Miguel, and P. S. Sahni, in *Phase Transitions and Critical Phenomena,* edited by C. Domb and J. L. Lebowitz (Academic, London, 1983), Vol. 8.
[2] K. Binder, in *Materials Science and Technology. Vol. 5. Phase Transformation in Materials,* edited by P. Haasen (VCH, Weinheim, 1990), p. 405.
[3] K. Binder, Ann. Phys. (N.Y.) **98**, 390 (1976); Phys. Rev. A **29**, 341 (1984); Physica (Amsterdam) **140A**, 35 (1986).
[4] K. Binder, in *Alloy Phase Stability,* edited by G. M. Stocks and A. Gonis (Kluwer Academic, Norwell, MA, 1989).
[5] D. Heerman, W. Klein, and D. Stauffer, Phys. Rev. Lett. **49**, 1262 (1982).
[6] A. Chakrabarti, Phys. Rev. B **45**, 9620 (1992).
[7] I. M. Lifshitz and V. V. Slyozov, J. Phys. Chem. Solids **19**, 35 (1961).
[8] D. A. Huse, Phys. Rev. B **34**, 7845 (1986).
[9] A. J. Bray, Phys. Rev. Lett. **62**, 2841 (1989).
[10] R. Toral, A. Chakrabarti, and J. D. Gunton, Phys. Rev. Lett. **60**, 2311 (1988); A. Chakrabarti, R. Toral, and J. D. Gunton, Phys. Rev. B **39**, 4386 (1989).
[11] T. M. Rogers, K. R. Elder, and R. C. Desai, Phys. Rev. B **37**, 9638 (1988).
[12] E. T. Gawlinski, J. Viñals, and J. D. Gunton, Phys. Rev. B **39**, 7266 (1989).
[13] K. Binder and D. Stauffer, Phys. Rev. Lett. **33**, 1006 (1974).
[14] J. L. Lebowitz, J. Marro, and M. H. Kalos, Acta Metall. **30**, 290 (1982), and references therein.
[15] J. W. Cahn and J. E. Hilliard, J. Chem. Phys. **28**, 258 (1958); H. E. Cook, Acta Metall. **18**, 297 (1970).
[16] T. M. Rogers and R. C. Desai, Phys. Rev. B **39**, 11 956 (1989).
[17] R. Toral, A. Chakrabarti, and J. D. Gunton, Phys. Rev. B **39**, 901 (1989).
[18] A. Chakrabarti, R. Toral, and J. D. Gunton, Phys. Rev. B **44**, 12 133 (1991).
[19] R. Toral, A. Chakrabarti, and J. D. Gunton, Phys. Rev. A **45**, R2147 (1992).
[20] M. Grant, M. San Miguel, J. Viñals, and J. D. Gunton, Phys. Rev. B **31**, 3027 (1985).
[21] See, for example, T. C. Gard, *Introduction to Stochastic Differential Equations* (Dekker, New York, 1988).
[22] M. Tokuyama, Y. Enomoto, and K. Kawasaki, Physica A **143**, 183 (1987).
[23] P. A. Rikvold and J. D. Gunton, Phys. Rev. Lett. **49**, 286 (1982).
[24] T. Ohta, Ann. Phys. (N.Y.) **158**, 31 (1984).
[25] H. Tomita, Prog. Theor. Phys. **71**, 1405 (1984).
[26] H. Furukawa, Prog. Theor. Phys. **74**, 174 (1985).
[27] P. Fratzl, J. L. Lebowitz, O. Penrose, and J. Amar, Phys. Rev. B **44**, 4794 (1991).
[28] G. F. Mazenko, Phys. Rev. Lett. **63**, 1605 (1989); Phys. Rev. B **43**, 5747 (1991).
[29] G. F. Mazenko (unpublished).
[30] P. Fratzl and J. L. Lebowitz, Acta Metall. **37**, 3245 (1989).
[31] P. Fratzl, J. Appl. Cryst. **24**, 593 (1991).
[32] G. Porod, in *Small-Angle X-Ray Scattering,* edited by O. Glatter and O. Kratky (Academic, London, 1983).
[33] The vertical and the horizontal scales are off by factors of 2 and $\sqrt{2}$, respectively, in the corresponding figures (Figs.

2 and 3) in Ref. [18].
[34] H. Furukawa, Physica A **123**, 497 (1984); J. Phys. Soc. Jpn. **58**, 216 (1989); Phys. Rev. Lett. **62**, 2567 (1989).
[35] C. Yeung, Phys. Rev. Lett. **61**, 1135 (1988).
[36] A. Chakrabarti, R. Toral, J. D. Gunton, and M. Muthukumar, J. Chem. Phys. **92**, 6899 (1990).
[37] T. Ohta and H. Nozaki, in *Space-Time Organization in Macromolecular Fluids,* edited by Fumihiko Tanaka, Masao Doi, and Takao Ohta, Springer Series in Chemical Physics Vol. 51 (Springer, Berlin, 1989).
[38] F. S. Bates and P. Wiltzius, J. Chem. Phys. **91**, 3258 (1989).
[39] A. Guinier and G. Fournet, *Small-Angle Scattering of X-Rays* (Wiley, New York, 1955).
[40] L. A. Feigin and D. I. Svergun, *Structure Analysis by Small-Angle X-Ray and Neutron Scattering* (Plenum, New York, 1987), Chap. II.
[41] A. J. Ardell, Phys. Rev. B **41**, 2554 (1990).
[42] A. J. Ardell, Acta Metall. **20**, 61 (1972).
[43] *Handbook of Mathematical Functions with Formulas, Graphs & Mathematical Tables,* edited by M. Abramowitz and I. A. Stegun (Dover, New York, 1964).
[44] J. A. Marqusee, J. Chem. Phys. **81**, 976 (1984).
[45] Q. Zheng and J. D. Gunton, Phys. Rev. A **39**, 4848 (1989).
[46] S. P. Marsh and M. E. Glicksman, in *Simulation and Theory of Evolving Microstructure,* edited by M. P. Anderson and A. D. Rollett (The Minerals, Metals and Materials Society, Warrendale, PA, 1990), p. 167.
[47] S. P. Marsh and M. E. Glicksman (unpublished).
[48] J. H. Yao, K. R. Elder, H. Guo, and M. Grant, Phys. Rev. B **45**, 8173 (1992); and (unpublished).
[49] Y. Oono and S. Puri, Phys. Rev. Lett. **58**, 863 (1987); A. Shinozaki and Y. Oono, *ibid.* **66**, 173 (1991).